Synthesis, Structure, and Characterization of N-Ligated $Mo_6S_8L_6$ Cluster Complexes. Molecular Precursors to Chevrel Phases

Shane J. Hilsenbeck, Victor G. Young, Jr.,† and Robert E. McCarley*

Ames Laboratory, USDOE, and Department of Chemistry, Iowa State University, Ames, Iowa 50011

Received November 12, 1993®

A modified method has been developed for the synthesis of the Mo_6S_8 cluster unit in one step from Mo_6Cl_{12} via reaction with NaSH and NaOBu in refluxing *n*-BuOH–pyridine. The ligand-deficient $Na_{2x}Mo_6S_{8+x}(py)_y$ (**1**) serves as a convenient starting material for the preparation of the amine complexes $Mo_6S_8L_6$, with L = pyridine (**2**), pyrrolidine (**4**), and piperidine (**5**). Although propylamine readily dissolves the ligand-deficient starting material, only amorphous $Mo_6S_8(PrNH_2)_{6-x}$ (**3**) could be isolated. However, the latter acts as a facile reactant for the preparation of the other complexes by ligand substitution. Crystallographic data for the complexes are as follows: $Mo_6S_8(py)_6 \cdot 2py$ (**2**), cubic, $Pa\bar{3}$, $a = 16.994(2)$ Å, $Z = 4$, $R = 0.0381$, $R_w = 0.0351$; $Mo_6S_8(pyrr)_6 \cdot pyrr$ (**4**), tetragonal, $I4_1/a$, $a = 29.933(4)$ Å, $c = 23.697(8)$ Å, $Z = 16$, $R = 0.0675$, wR2 = 0.2034; $Mo_6S_8(pip)_6 \cdot 7pip$, (**5**), tetragonal, $I\bar{4}$, $a = 19.421(2)$ Å, $c = 22.584(3)$ Å, $Z = 8$, $R = 0.0317$, $R_w = 0.0366$. These complexes all show strong bands in the IR at 380 ± 5 cm^{-1} and in the Raman at 414 ± 4 cm^{-1}, assigned as predominantly Mo–S stretching modes. XP spectra give characteristic binding energies at 227.7 ± 0.1 (Mo $3d_{5/2}$), 230.8 ± 0.1 (Mo $3d_{3/2}$), 225.1 ± 0.3 (S 2s), 160.6 ± 0.1 (S $2p_{3/2}$), and 161.8 ± 0.1 (S $2p_{1/2}$) eV. Mo–Mo and Mo–S bond distances show little variation among the complexes, with average values of 2.647 and 2.454 Å, respectively. The average Mo–N bond distance, 2.297 Å, indicates rather weak bonding of these N-donor ligands.

Introduction

Ternary molybdenum chalcogenides of the general formula $M_xMo_6Y_8$ (M = ternary metal cation; Y = chalcogenide), known as Chevrel phases, have been extensively studied and have been shown to include superconductors with high H_{c2},[1] ordered magnetic phases,[2] solid electrolytes (fast ion conductors),[3] and hydrodesulfurization (HDS) catalysts.[4] These properties are related to the structures of the compounds which consist of Mo_6Y_8 clusters interlinked to form three-dimensional networks. The production of the Chevrel phases has generally involved solid-state reactions at higher temperatures (1000–1300 °C). Recently, though, lower temperature routes via solution precursors were sought so that films, coatings, and small particles, either by themselves or on typical catalyst support materials, can be prepared.[5] The structural similarity of Mo_6Cl_{12} to the Chevrel phases prompted its use as a starting complex.[6,7] This similarity is evidenced in that both materials possess a Mo_6X_8 (X = Cl or S) octahedral cluster unit. Complete substitution of sulfide for chloride was successfully accomplished without cluster decomposition.[8] Further reaction of this pyridine complex has led to the preparation and structural characterization of molecular complexes $Mo_6S_8L_6$, where L is an organic donor ligand such as triethylphosphine or tetrahydrothiophene.[8] Concurrently, the triethylphosphine adduct was prepared by another synthetic route.[9]

The present paper describes an improved method for the preparation of the initial sulfide cluster compound, $Na_{2x}Mo_6S_{8+x}(py)_y$. The syntheses, characterizations, and structures of new nitrogen donor complexes which are produced from this cluster compound are then described.

Experimental Section

Materials. The reagents and products are air and moisture sensitive. Therefore, all manipulations were performed by the use of an inert-atmosphere drybox, a high-vacuum manifold, and Schlenk techniques, unless otherwise stated. Mo_6Cl_{12} was prepared by the high-temperature conproportionation method described by Koknat *et al.*[10] Anhydrous sodium hydrosulfide (NaSH) was prepared by the reaction of hydrogen sulfide with sodium ethoxide by using the procedure described by Brauer.[11] Sodium butoxide (NaOBu) was prepared by the reaction of 1-butanol with sodium metal and used as the solid. All solvents were purified and dried prior to use and then distilled onto 3- or 4-Å molecular sieves and stored under vacuum or a nitrogen atmosphere. Pyridine (Fisher), *n*-propylamine (Aldrich), pyrrolidine (Aldrich), and piperidine (Fisher) were purified by refluxing over calcium hydride for at least 4 h. Without heating, 1-butanol (Fisher) was stirred with sodium metal. Methanol (Mallinckrodt) was dried by refluxing over sodium methoxide.

Physical Measurements. Infrared spectra (4000–200 cm^{-1}) were recorded with a Bomem MB-102 Fourier transform infrared spectrometer equipped with CsI optics. Samples were prepared as Nujol mulls and mounted between CsI windows. Raman spectra were obtained with a Spex Triplemate spectrometer with a PARC intensified SiPD detector cooled to −40 °C. The excitation source was a Coherent Ar^+ 200 series laser at the wavelength of 514.5 nm, and the scattered radiation was collected in a backscattering geometry. The laser power at the sample was approximately 20 mW, and the integration time was 200 s. The Raman spectra were obtained at liquid nitrogen temperatures from solid samples packed in capillary tubes. ^1H NMR spectra were collected on a Unity 500-MHz spectrometer with the samples dissolved in deuterated benzene. Two-dimensional NMR experiments—double quantum correlation spectroscopy (DQCOSY) and nuclear Overhauser effect spectroscopy (NOESY)—were also performed. XP spectra were collected

† Iowa State University Molecular Structure Laboratory.

® Abstract published in *Advance ACS Abstracts*, April 1, 1994.

(1) Chevrel, R.; Sergent, M. *Topics in Current Physics*, Fischer, Ø., Maple, M. B., Eds.; Springer-Verlag: Heidelberg, Germany, 1982; Vol. 32, Chapter 2.
(2) Peña, O.; Sergent, M. *Prog. Solid State Chem.* **1989**, *19*, 165.
(3) Mulhern, P. J.; Haering, R. R. *Can. J. Phys.* **1984**, *62*, 527.
(4) (a) McCarty, K. F.; Schrader, G. L. *Ind. Eng. Chem. Prod. Res. Dev.* **1984**, *23*, 519. (b) McCarty, K. F.; Anderegg, J. W.; Schrader, G. L. *J. Catal.* **1985**, *93*, 375.
(5) (a) Nanjundaswamy, K. S.; Vasanthacharya, N. Y.; Gopalakrishnan, J.; Rao, C. N. R. *Inorg. Chem.* **1987**, *26*, 4286. (b) Rabiller-Baudry, M.; Sergent, M.; Chevrel, R. *Mater. Res. Bull.* **1991**, *26*, 519.
(6) Michel, J. B. Ph.D. Dissertation, Iowa State University, Ames, IA, 1979.
(7) Laughlin, S. K. Master's Thesis, Iowa State University, Ames, IA, 1986.
(8) (a) McCarley, R. E.; Laughlin, S. K.; Spink, D. A.; Hur, N. *Abstracts of Papers*, 3rd Chemical Congress of North America, Toronto, Ontario, Canada, 1988; American Chemical Society: Washington, DC, 1988. (b) Zhang, X.; Hur, N.; Spink, D. A.; Michel, J. B.; Laughlin, S. K.; McCarley, R. E. Manuscript in preparation.
(9) Saito, T.; Yamamoto, N.; Yamagata, T.; Imoto, H. *J. Am. Chem. Soc.* **1988**, *110*, 1646.
(10) Koknat, F. W.; Adaway, T. J.; Erzerum, S. I.; Syed, S. *Inorg. Nucl. Chem. Lett.* **1980**, *16*, 307.
(11) Brauer, G. *Handbuch der Preparativen Anorganischen Chemie*; Ferdinand Enke Verlag: Stuttgart, Germany, 1975; p 371.

0020-1669/94/1333-1822$04.50/0

with a Physical Electronics Industries 5500 multitechnique surface analysis system, and the binding energies were calibrated with C 1s = 284.6 eV. Powder X-ray diffraction data were obtained with an Enraf-Nonius Delft FR552 Guinier camera using Cu Kα radiation. The air-sensitive samples were placed between strips of cellophane tape in the drybox, and silicon was added as an internal standard.

Chemical Analyses. Molybdenum was determined gravimetrically as the 8-hydroxyquinolate.[12] Chlorine was determined by potentiometric titration with a standardized silver nitrate solution. Additional microanalyses for carbon, hydrogen, nitrogen, and sodium were obtained from Oneida Research Services.[13]

Preparation of $Na_{2x}Mo_6S_{8+x}(py)_y$ (1). Mo_6Cl_{12} (4.00 g, 4 mmol), NaSH (2.69 g, 48 mmol), and NaOBu (2.30 g, 24 mmol) were weighed in the drybox and transferred to a Schlenk reaction flask equipped with a water-cooled condenser. By syringe, 60 mL of 1-butanol and 15 mL of pyridine were added to the reactants. The mixture was then refluxed for 2–4 days. After cooling, a dark brown solid and faint-colored solution were separated by filtration. The solid was extracted with methanol for several days to remove the NaCl byproduct, and the remaining solid was dried *in vacuo*. The resulting brown/black solid (3.92 g, 93%) showed no evidence of Cl by chlorine analyses. However, further study of this product by XPS indicated that sodium was present. Also, it was discovered that the pyridine and methanol contents were variable from one reaction to another. The pyridine-deficient product was found to be pyrophoric, insoluble in noncoordinating solvents, and amorphous to X-rays. IR (Nujol, cm^{-1}): 1597 (vw), 1213 (vw), 750 (vw), 690 (vw), Mo–S 392 (s, br). Anal. Calcd for $Na_{0.8}Mo_6S_{8.4}(py)_2(MeOH)$: Na, 1.75; Mo, 54.64; C, 12.54; H, 1.34; N, 2.66. Found: Na, 1.73; Mo, 54.55; C, 12.67; H, 1.44; N, 2.27.

Preparation of $Mo_6S_8(py)_6$ (2). The pyridine-deficient compound (1) was reacted in neat pyridine either at room temperature or under reflux conditions to produce a more highly pyridine-coordinated material. A typical preparation involved the placement of 1.00 g of the pyridine-deficient compound into a 100-mL Schlenk reaction flask and the syringing of 30 mL of pyridine onto the solids under a nitrogen flow. The mixture was refluxed for 1–2 days or stirred for 3–4 days, and the result, after filtration, was a dark brown solid and a brownish solution. The solid was found to contain sodium as detected by XPS. IR of brown solid (Nujol, cm^{-1}): 1589 (m), 1570 (w), 1477 (w, sh), 1441 (ms), 1213 (vw), 1148 (w), 1067 (m), 1038 (m), 1009 (vw), 752 (ms), 690 (m), 629 (w), 612 (w), 430 (w), Mo–S 378 (s). Anal. Calcd for brown solid on frit, $Na_{1.5}Mo_6S_{8.75}(py)_6$: Na, 2.53; Mo, 42.16; C, 26.39; H, 2.21; N, 6.16. Found: Na, 2.15; Mo, 41.88; C, 23.42; H, 2.00; N, 5.41.

Crystals of $Mo_6S_8(py)_6$ were grown from the brownish solution by reducing the volume and placing it in a refrigerator for several days. This material did not contain sodium, as indicated by a negative flame test. Subsequent crystallographic work showed that two polymorphs of $Mo_6S_8(py)_6$·2py were present.

Preparation of $Mo_6S_8(PrNH_2)_{6-x}$ (3). The pyridine-deficient compound (1) was nearly quantitatively converted to 3 by extraction with neat *n*-propylamine. A typical preparation involved the placement of 2.0–3.0 g of $Na_{2x}Mo_6S_{8+x}(py)_y$ onto the frit of an extractor and the distillation of 25–30 mL of *n*-propylamine ($PrNH_2$) into the receiving flask. After approximately 4–6 h of extraction, the solid completely dissolved and provided a dark black/brown solution. After the sample was dried under dynamic vacuum, a black solid was obtained. This product, $Mo_6S_8(PrNH_2)_{6-x}$, showed variable propylamine content, which was dependent upon the amount of drying. Also, the propylamine adduct was amorphous to X-rays and insoluble in noncoordinating solvents. IR (Nujol, cm^{-1}): 3170 (vw), 1568 (m), 1477 (w, sh), 1213 (vw), 1066 (vw), 1038 (m), 997 (m), 962 (mw), 860 (vw), 750 (w), 627 (w), Mo–S 384 (s, br).

Preparation of $Mo_6S_8(pyrr)_6$ (4). The propylamine adduct (3, 0.50 g) was weighed in the drybox and transferred into a 100-mL Schlenk reaction flask, and 25–30 mL of pyrrolidine (pyrr) was vacuum-distilled onto the solid. After the mixture was refluxed for 1 day or stirred at room temperature for 2–3 days, the solid completely dissolved and a red/brown solid was obtained upon filtration and drying. The pyrrolidine content was found to be variable depending upon reaction and drying conditions. The pyrrolidine adduct was soluble in toluene and benzene. A small quantity of single crystals was grown by layering the filtrate with diethyl ether and allowing it to stand at room temperature for several days. IR (Nujol, cm^{-1}): 3194 (m), 1583 (w), 1303 (w), 1225 (w), 1209 (w), 1070 (s), 1029 (s), 940 (m), 904 (s), 656 (w), 522 (vw), Mo–S 381 (s). Anal. Calcd for $Mo_6S_8(pyrr)_{5.3}$: Mo, 47.61; C, 21.06; H, 3.98; N, 6.14. Found: Mo, 47.55; C, 20.74; H, 3.94; N, 5.60.

Preparation of $Mo_6S_8(pip)_6$ (5). The propylamine adduct (3, 0.30–0.50 g) was weighed in the drybox and transferred into a 100-mL Schlenk reaction flask, and 25–30 mL of piperidine (pip) was vacuum-distilled onto the solid. After 1 day of refluxing or 2–3 days of stirring at room temperature, the solid completely dissolved, resulting in a red solid upon filtration and drying. The piperidine content was also found to be variable depending upon reaction and drying conditions. The piperidine adduct was soluble in toluene, benzene, and chlorobenzene. Single crystals were grown by slowly reducing the volume of the filtrate and allowing it to stand at room temperature for several days. IR (Nujol, cm^{-1}): 3214 (w), 1593 (w, br), 1311 (w), 1188 (w), 1169 (w), 1084 (w), 1045 (m), 1018 (s), 971 (s), 940 (w), 869 (s), 807 (ms), 739 (w), 627 (w), 597 (w), Mo–S 382 (s). Anal. Calcd for $Mo_6S_8(pip)_6$·pip: Mo, 40.31; C, 29.44; H, 5.43; N, 6.87. Found: Mo, 39.53; C, 25.73; H, 5.15, N, 5.70. Anal. Calcd for sample used for NMR study, $Mo_6S_8(pip)_6$·6pip: Mo, 31.05; C, 38.87; H, 7.18; N, 9.07. Found: Mo, 29.66; C, 34.06; H, 6.21; N, 7.52. ^1H NMR (C_6D_6): δ 0.86 ppm, β-CH_aH_e (ddddd, $^2J_{GD}$ = 12.5 Hz, $^3J_{GA}$ = 13.6 Hz, $^3J_{GB}$ = 12.5 Hz, $^3J_{GE}$ = 3.6 Hz, $^3J_{GF}$ = 12.5 Hz, 12H); δ 1.01 ppm, γ-CH_aH_e (dtt, $^2J_{FE}$ = 12.5 Hz, $^3J_{FD}$ = 3.5 Hz, $^3J_{FG}$ = 12.5 Hz, 6H); δ 1.12 ppm, γ-CH$_a$H$_e$ (dtt, $^2J_{EF}$ = 13.0 Hz, $^3J_{ED}$ = 1.8 Hz, $^3J_{EG}$ = 3.6 Hz, 6H); δ 1.33 ppm, β-CH$_a$H$_e$ (d, $^2J_{DG}$ = 12.5 Hz, ^3J couplings not resolved, 12H); δ 3.09 ppm, N–H$_a$, (tt, $^3J_{CB}$ = 11.4 Hz, $^3J_{CA}$ not resolved, 6H); δ 3.19 ppm, α-CH_aH_e (dddd, $^2J_{BA}$ = 11.7 Hz, $^3J_{BC}$ = 11.7 Hz, $^3J_{BD}$ = 2.7 Hz, $^3J_{BG}$ = 11.7 Hz, 12H); δ 3.88 ppm, α-CH$_a$H$_e$ (d, $^2J_{AB}$ = 12.5 Hz, ^3J couplings not resolved, 12H).

X-ray Structure Determinations

Single-crystal structure determinations were undertaken for the pyridine, pyrrolidine, and piperidine adducts. In each case, a crystal was chosen while in contact with the mother solution. The crystal was encased in Paratone oil, attached to the tip of a glass fiber, and immediately inserted into the low-temperature nitrogen stream of the Siemens P4/RA diffractometer for data collection. The cell constants were determined from reflections found by a rotation photograph. A nonlinear correction based on the decay in the standard reflections was applied to the data. Lorentz and polarization corrections were also applied. The refinement calculations were performed on a Digital Equipment Corp. Micro VAX 3100/76 computer using SHELXTL-PLUS programs.[14a] Further refinement of the pyrrolidine adduct was explored with SHELXL-93.[14b] Pertinent crystallographic data are listed in Table 1.

$Mo_6S_8(py)_6$·2py (2). A brown cubic crystal, with dimensions of 0.12 × 0.12 × 0.12 mm, was attached to the tip of a glass fiber, and data collection proceeded at −45 ± 1 °C. Graphite-monochromated Mo radiation was employed to collect data in the range $4° < 2\theta < 55°$, using the θ–2θ scan technique. A total of 1460 unique reflections were collected, of which 695 were considered as observed with $F > 6.0\sigma(F)$. The agreement factor for the averaging of reflections was 3.81%.

The cubic space group $Pa\bar{3}$ was chosen on the basis of systematic absences and intensity statistics. All non-hydrogen atoms were placed directly from the electron density difference map and were refined with anisotropic thermal parameters. The hydrogens of the coordinated pyridines were refined as riding atoms with an ideal distance of 0.96 Å from the host atom and with individual isotropic thermal parameters. The one solvent molecule was disordered about a 3-fold axis (8c site symmetry). All sites were modeled to account for this disorder by refining each position as $^5/_6$th carbon and $^1/_6$th nitrogen. The atomic coordinates and equivalent isotropic thermal parameters of the non-hydrogen atoms are given in Table 2.

A triclinic polymorph with the composition $Mo_6S_8(py)_6$·2py was also found: $P\bar{1}$, a = 11.580(5) Å, b = 12.170(6) Å, c = 21.995(9) Å, α = 75.94(3)°, β = 88.94(3)°, γ = 62.61(3)°, Z = 2. However, solvent loss resulted in a less than ideal structure refinement (R = 0.075, R_w = 0.094).

$Mo_6S_8(pyrr)_6$·pyrr (4). A reddish-brown, rectangular crystal, with dimensions of 0.45 × 0.40 × 0.12 mm, was attached to the tip of a glass fiber for data collection at −60 ± 1 °C. Graphite-monochromated Cu radiation (λ 1.541 78 Å) was employed to collect data in the range $4° < 2\theta < 115°$, using the θ–2θ scan technique. A total of 7147 unique reflections were collected, of which 4168 were considered as observed

(12) Elwell, W. T.; Wood, D. F. *Analytical Chemistry of Molybdenum and Tungsten*; Pergamon Press: New York, 1971.
(13) Oneida Research Services, Inc., Whitesboro, NY.
(14) (a) SHELXTL-PLUS, Siemens Analytical Xray, Inc., Madison, WI. (b) Sheldrick, G. M. SHELXL-93. *J. Appl. Crystallogr.* in press.

Table 1. Summary of Crystallographic Data for the $Mo_6S_8L_6$ Cluster Complexes

compound	$Mo_6S_8(py)_6 \cdot 2py$ (2)	$Mo_6S_8(pyrr)_6 \cdot pyrr$ (4)	$Mo_6S_8(pip)_6 \cdot 7pip$ (5)
chem formula	$C_{40}H_{40}Mo_6N_8S_8$	$C_{28}H_{63}Mo_6N_7S_8$	$C_{65}H_{143}Mo_6N_{13}S_8$
fw	1464.9	1330.0	1939.1
space group	$Pa\bar{3}$ (No. 205)	$I4_1/a$ (No. 88)	$I\bar{4}$ (No. 82)
a, Å	16.994(2)	29.933(4)	19.421(2)
c, Å		23.697(8)	22.584(3)
V, Å^3	4908(1)	21 232(8)	8518(2)
Z	4	16	8
ρ_{calcd}, g/cm^3	1.980	1.575	1.510
μ, cm^{-1}	0.1865	1.4362	0.1096
radiation (λ, Å)	Mo Kα (0.710 73)	Cu Kα (1.541 78)	Mo Kα (0.710 73)
T, °C	−45	−60	−50
R^a	0.0381	0.0675	0.0317
R_w,[b] wR2[c]	0.0351[b]	0.2034[c]	0.0366[b]

[a] $R = \sum||F_o| - |F_c||/\sum|F_o|$. [b] $R_w = [\sum w(|F_o| - |F_c|)^2/\sum w|F_o|^2]^{1/2}$; $w = 1/\sigma^2(|F_o|)$. [c] $wR2 = [\sum(w(F_o^2 - F_c^2)^2)/\sum(w(F_o^2)^2)]^{1/2}$; $w = 1/[\sigma^2(F_o^2) + (0.141P)^2 + 0.00P]$; $P = [\max(F_o^2) + 2F_c]/3$.

Table 2. Atomic Coordinates and Equivalent Isotropic Thermal Parameters (Å^2) of the Non-Hydrogen Atoms for $Mo_6S_8(py)_6 \cdot 2py$

atom	x	y	z	U_{eq}[a]
Mo	0.0578(1)	0.5870(1)	0.0345(1)	0.034(1)
S(1)	0.1025(2)	−0.3975(2)	−0.1025(2)	0.045(1)
S(2)	0.1665(2)	0.4942(2)	0.0598(2)	0.041(1)
N	0.1279(6)	0.6934(5)	0.0771(5)	0.044(3)
C(1)	0.0959(8)	0.7485(7)	0.1235(8)	0.063(5)
C(2)	0.1355(10)	0.8098(8)	0.1533(9)	0.080(6)
C(3)	0.2115(11)	0.8169(8)	0.1387(10)	0.099(8)
C(4)	0.2478(9)	0.7641(9)	0.0901(9)	0.087(7)
C(5)	0.2036(8)	0.7016(8)	0.0624(7)	0.063(5)
C(11)[b]	0.3851(14)	0.5076(14)	0.0749(20)	0.169(14)
N(11)[b]	0.3851(14)	0.5076(14)	0.0749(20)	0.169(14)
C(12)[b]	0.4408(19)	0.5194(19)	0.1225(11)	0.147(14)
N(12)[b]	0.4408(19)	0.5194(19)	0.1225(11)	0.147(14)

[a] Equivalent isotropic U defined as one-third of the trace of the orthogonalized U_{ij} tensor ($U_{eq} = {}^1/_3\sum_i\sum_j U_{ij}a_i^*a_j^*a_ia_j$). [b] Disordered positions.

with $F > 4.0\sigma(F)$. A semiempirical absorption correction was applied, resulting in transmission factors ranging from 0.008 to 0.200. The agreement factor for the averaging of reflections was 6.44%.

The tetragonal space group $I4_1/a$ was chosen on the basis of systematic absences. The Mo, S, and N atoms were placed directly from the electron density difference map. The carbons were refined as isotropic atoms; however, all of the N–C and C–C bonds were constrained to reasonable distances. Modeling in this manner revealed envelope-flap type disorder in each of the coordinated pyrrolidine rings. One solvent pyrrolidine was also observed. The structure was composed of two half-molecules that were related by symmetry. The Mo, S, and N atoms were refined with anisotropic thermal parameters. The observed disorder arose from the flexing of individual pyrrolidine rings. Solvent loss also affected the quality of this refinement. No hydrogen atoms were located or placed for this complex. The atomic coordinates and equivalent isotropic thermal parameters of the non-hydrogen atoms are listed in Table 3.

$Mo_6S_8(pip)_6 \cdot 7pip$ (5). An irregularly shaped reddish-brown crystal, with dimensions of 0.50 × 0.40 × 0.35 mm, was attached to the tip of a glass fiber for data collection at −50 ± 1 °C. Graphite-monochromated Mo radiation (λ 0.710 73 Å) was employed to collect data in the range $4° < 2\theta < 60°$, using the θ–2θ scan technique. A total of 6713 unique reflections were collected, of which 5008 were considered as observed with $F > 6.0\sigma(F)$. A semiempirical absorption correction was applied, resulting in transmission factors ranging from 0.7307 to 0.8647. The agreement factor for the averaging of reflections was 2.16%.

The tetragonal space group $I\bar{4}$ was chosen on the basis of systematic absences and intensity statistics. All non-hydrogen atoms were placed directly from the electron density difference map. These atoms were refined with anisotropic thermal parameters, except for those of the disordered piperidine solvent molecule. The hydrogens of the coordinated piperidines were refined as riding atoms with C–H distances equal to 0.96 Å, with N–H distances of 0.85 Å, and with fixed isotropic thermal parameters. The asymmetric unit was found to be $Mo_3S_4(pip)_3 \cdot 3.5pip$, where three of the solvent piperidine molecules were well-behaved, but the remaining half-piperidine molecule was disordered. This disorder occurred about a crystallographic 2-fold axis and was modeled with atoms C(71), N(71), C(72), N(72), C(73), and N(73). The carbon/nitrogen atoms of this solvent molecule were given occupancies with the 0.833:0.167 ratio. Hydrogen atoms were placed with an occupancy of 0.833. These C–C and C–N bond lengths were constrained to be 1.5200(1) Å in order to approach convergence. Thermal parameters of like atoms were constrained to have the same value.

The three ligand piperidine groups were found in the chair conformation. Likewise, the three well-behaved solvent piperidine molecules were also in the chair conformation. However, the disordered piperidine molecule, once joined with its symmetry equivalent, displayed the boat conformation. The atomic coordinates and equivalent isotropic thermal parameters of the non-hydrogen atoms are given in Table 4.

The large, highly anisotropic thermal parameters of the ligand carbon atoms suggested that torsional motion was involved. Consequently, a librational analysis was performed for all three piperidine ligands. R_G values of 7–8% were found for the Schomaker–Trueblood fit to a rigid body.[15] This result suggested that flexing of the chair conformation contributes to the thermal displacements at least as much as the rigid-body motion.

Results and Discussion

Syntheses. (a) Sulfidation Reactions. Previous research on sulfide substitution into the $Mo_6Cl_8^{4+}$ cluster units (Mo_6Cl_{12}) showed that NaSH was a good sulfiding agent.[6] In addition, the use of a proton acceptor (OBu^-) in 1-butanol led to greater and more facile sulfide substitution.[7] The completely sulfided Mo_6S_8 cluster compound has previously been prepared by the following two-step reaction sequence:[8]

$$Mo_6Cl_{12} + 8NaSH + 4NaOBu \xrightarrow[\text{reflux, 3d}]{\text{BuOH/py}} \xrightarrow[\text{4 days}]{\text{MeOH}} \text{“}Mo_6S_7Cl(py)_x\text{”}$$

$$\text{“}Mo_6S_7Cl(py)_x\text{”} + 2NaSH \xrightarrow[\text{reflux, 3d}]{\text{BuOH/py}} \xrightarrow[\text{4 days}]{\text{MeOH}} \text{“}Mo_6S_8(py)_{\sim 4}\text{”}$$

On the basis of the observation that an excess of sulfiding agent was needed in order to produce a completely sulfur-substituted product, research into reactions with a higher sodium hydrosulfide content was initiated. When the reaction stoichiometry was increased to 1:12:6 (Mo_6Cl_{12}:NaSH:NaOBu), a one-step procedure for the preparation of the Mo_6S_8 cluster unit resulted. The brown/black product is highly pyridine deficient, as indicated by the weak pyridine coordination bands evidenced at 1597, 1213, 750, and 690 cm^{-1} and low elemental analyses for C and N. A broad Mo–S stretching mode is centered at about 392 cm^{-1}. Examination of this compound by XPS indicates the presence of sodium and absence of chlorine, which shows that sodium is not present as NaCl. Likewise, no evidence is found for cluster reduction and formation of $Na_xMo_6S_8(py)_y$ or for the presence of trapped Na_2S. Further work has shown the ability

(15) Schomaker, V.; Trueblood, K. N. *Acta Crystallogr.* **1968**, *B24*, 63.

Table 3. Atomic Coordinates and Equivalent Isotropic Thermal Parameters (Å²) of the Non-Hydrogen Atoms for $Mo_6S_8(pyrr)_6 \cdot pyrr$

atom	x	y	z	U_{eq}[a]
Mo(11)	0.0242(1)	0.2868(1)	−0.0033(1)	0.055(1)
Mo(12)	0.0252(1)	0.2869(1)	−0.1149(1)	0.054(1)
Mo(13)	0.0520(1)	0.2150(1)	−0.0598(1)	0.055(1)
Mo(21)	0.4798(1)	0.5584(1)	0.0132(1)	0.061(1)
Mo(22)	0.4786(1)	0.4828(1)	0.0711(1)	0.066(1)
Mo(23)	0.4449(1)	0.4856(1)	−0.0319(1)	0.068(1)
S(11)	−0.0025(1)	0.3496(1)	−0.0596(1)	0.064(1)
S(12)	0.0939(1)	0.2850(1)	−0.0585(1)	0.063(1)
S(13)	−0.0484(1)	0.2818(1)	0.0433(1)	0.064(1)
S(14)	−0.0473(1)	0.2820(1)	−0.1632(1)	0.065(1)
S(21)	0.5124(2)	0.5511(1)	0.1075(2)	0.085(1)
S(22)	0.5495(1)	0.4433(1)	0.0831(2)	0.077(1)
S(23)	0.4479(1)	0.4168(1)	0.0244(2)	0.079(1)
S(24)	0.4110(1)	0.5246(1)	0.0481(2)	0.084(1)
N(11)	0.0500(4)	0.3290(4)	0.0698(5)	0.078(3)
C(111)	0.1000(5)	0.3345(8)	0.0787(10)	0.146(8)
C(112)[b]	0.0984(15)	0.3801(10)	0.0459(17)	0.148(17)
C(115)[b]	0.1036(14)	0.3818(10)	0.1074(17)	0.131(15)
C(113)	0.0639(10)	0.4083(11)	0.0805(18)	0.296(22)
C(114)	0.0252(7)	0.3728(6)	0.0780(9)	0.130(7)
N(12)	0.0598(4)	0.3307(3)	−0.1796(4)	0.073(3)
C(121)	0.0779(6)	0.3744(5)	−0.1571(7)	0.095(5)
C(122)	0.0764(12)	0.4059(9)	−0.2096(10)	0.227(15)
C(123)[b]	0.0580(11)	0.3799(9)	−0.2624(12)	0.106(11)
C(125)[b]	0.0263(12)	0.3895(11)	−0.2104(30)	0.245(33)
C(124)	0.0328(6)	0.3405(6)	−0.2327(7)	0.105(6)
N(13)	0.1172(4)	0.1746(4)	−0.0654(5)	0.079(4)
C(131)	0.1105(8)	0.1279(6)	−0.0895(10)	0.140(8)
C(132)[b]	0.1499(11)	0.1036(11)	−0.0581(15)	0.256(18)
C(133)	0.1795(10)	0.1355(10)	−0.0214(16)	0.115(12)
C(135)[b]	0.1287(17)	0.1266(11)	−0.0051(19)	0.181(23)
C(134)	0.1466(8)	0.1754(9)	−0.0130(8)	0.165(10)
N(21)	0.4573(4)	0.6309(4)	0.0235(5)	0.074(3)
C(211)	0.4079(5)	0.6375(7)	0.0343(10)	0.132(8)
C(212)	0.4175(11)	0.6599(12)	0.0922(12)	0.251(17)
C(213)[b]	0.4650(10)	0.6585(14)	0.1200(10)	0.121(13)
C(215)[b]	0.4536(10)	0.6966(9)	0.0797(18)	0.121(13)
C(214)	0.4870(5)	0.6592(5)	0.0603(7)	0.092(5)
N(22)	0.4546(5)	0.4585(4)	0.1565(6)	0.096(4)
C(221)	0.4046(6)	0.4565(9)	0.1677(10)	0.167(10)
C(222)[b]	0.3953(12)	0.4561(14)	0.2329(11)	0.105(12)
C(226)[b]	0.4191(19)	0.4673(22)	0.2303(13)	0.183(23)
C(223)[b]	0.4610(15)	0.4605(22)	0.2694(14)	0.166(25)
C(225)[b]	0.4425(12)	0.4644(18)	0.2593(14)	0.116(14)
C(224)	0.4740(8)	0.4791(8)	0.2097(8)	0.161(9)
N(23)	0.3745(5)	0.4703(7)	−0.0706(8)	0.149(7)
C(231)	0.3667(14)	0.4727(14)	−0.1335(9)	0.269(19)
C(232)	0.3163(14)	0.4602(15)	−0.1419(18)	0.288(22)
C(233)	0.3068(13)	0.4467(15)	−0.0789(18)	0.288(21)
C(234)[b]	0.3522(13)	0.4257(9)	−0.0597(20)	0.138(16)
C(235)[b]	0.3382(7)	0.4611(9)	−0.0273(10)	0.117(13)
C(301)	0.7463(7)	0.4050(9)	0.1313(10)	0.333(49)
C(302)	0.7324(7)	0.3470(9)	0.1076(10)	0.182(22)
C(303)	0.7069(7)	0.3046(9)	0.0654(10)	0.233(31)
C(304)	0.7013(7)	0.3512(9)	0.0276(10)	0.176(21)
C(305)	0.7217(7)	0.4088(9)	0.0594(10)	0.211(27)

[a] Equivalent isotropic U defined as one-third of the trace of the orthogonalized U_{ij} tensor ($U_{eq} = {}^1/_3\sum_i\sum_j U_{ij}a_i^*a_j^*a_ia_j$). [b] Atoms disordered over two sites and positions refined at 0.50 occupancy.

Table 4. Atomic Coordinates and Equivalent Isotropic Thermal Parameters (Å²) of the Non-Hydrogen Atoms for $Mo_6S_8(pip)_6 \cdot 7pip$

atom	x	y	z	U_{eq}[a]
Mo(1)	0.4925(1)	0.5961(1)	0.2664(1)	0.019(1)
Mo(2)	0.4323(1)	0.4947(1)	0.2071(1)	0.019(1)
Mo(3)	0.4319(1)	0.4951(1)	0.3248(1)	0.019(1)
S(1)	0.4937(1)	0.5900(1)	0.1581(1)	0.024(1)
S(2)	0.3809(1)	0.4018(1)	0.2662(1)	0.024(1)
S(3)	0.4943(1)	0.5879(1)	0.3744(1)	0.025(1)
S(4)	0.3671(1)	0.5795(1)	0.2660(1)	0.023(1)
N(1)	0.4753(2)	0.7144(2)	0.2624(3)	0.028(1)
C(11)	0.5289(3)	0.7531(3)	0.2320(4)	0.044(2)
C(12)	0.5114(4)	0.8299(3)	0.2251(4)	0.053(3)
C(13)	0.4963(5)	0.8261(4)	0.2826(4)	0.069(4)
C(14)	0.4397(5)	0.8224(4)	0.3144(4)	0.065(4)
C(15)	0.4587(5)	0.7456(4)	0.3193(4)	0.056(3)
N(2)	0.3531(3)	0.4816(3)	0.1310(2)	0.025(1)
C(21)	0.3780(3)	0.5029(4)	0.0729(3)	0.036(2)
C(22)	0.3307(4)	0.4833(5)	0.0217(3)	0.052(3)
C(23)	0.2590(5)	0.5142(5)	0.0325(4)	0.064(3)
C(24)	0.2327(4)	0.4908(5)	0.0929(3)	0.055(3)
C(25)	0.2834(3)	0.5094(4)	0.1421(3)	0.044(2)
N(3)	0.3456(3)	0.4902(3)	0.3949(2)	0.028(2)
C(31)	0.3385(5)	0.5498(5)	0.4320(4)	0.076(4)
C(32)	0.2740(5)	0.5446(6)	0.4728(5)	0.095(5)
C(33)	0.2723(5)	0.4798(9)	0.5091(4)	0.117(7)
C(34)	0.2806(6)	0.4231(7)	0.4700(5)	0.106(6)
C(35)	0.3458(4)	0.4257(5)	0.4304(4)	0.075(4)
N(4)	0.3325(4)	0.3205(3)	0.1369(3)	0.056(2)
C(41)	0.3571(6)	0.2771(7)	0.0910(5)	0.103(5)
C(42)	0.3082(7)	0.2490(9)	0.0540(5)	0.144(8)
C(43)	0.2482(6)	0.2190(6)	0.0834(5)	0.099(5)
C(44)	0.2253(7)	0.2621(9)	0.1347(7)	0.166(9)
C(45)	0.2709(7)	0.2920(7)	0.1657(6)	0.143(7)
N(5)	−0.0226(4)	0.2757(3)	0.1930(3)	0.048(2)
C(51)	−0.0883(5)	0.3074(4)	0.2052(5)	0.068(4)
C(52)	−0.1000(5)	0.3680(4)	0.1628(5)	0.065(3)
C(53)	−0.0417(5)	0.4184(4)	0.1686(4)	0.055(3)
C(54)	0.0272(5)	0.3821(5)	0.1623(5)	0.069(4)
C(55)	0.0321(5)	0.3218(4)	0.2037(5)	0.066(3)
N(6)	0.6418(3)	0.2881(3)	0.1626(3)	0.038(2)
C(61)	0.7124(4)	0.2751(4)	0.1757(4)	0.051(3)
C(62)	0.7294(5)	0.2017(5)	0.1673(5)	0.067(3)
C(63)	0.7130(5)	0.1778(5)	0.1053(4)	0.070(4)
C(64)	0.6414(5)	0.1986(5)	0.0882(4)	0.071(4)
C(65)	0.6265(4)	0.2737(5)	0.1002(3)	0.057(3)
C(71)[b]	0.5620(13)	0.0202(12)	0.0392(12)	0.0252(13)
N(71)[b]	0.5620(13)	0.0202(12)	0.0392(12)	0.0252(13)
C(72)[b]	0.5422(12)	−0.0556(12)	0.0403(9)	0.197(9)
N(72)[b]	0.5422(12)	−0.0556(12)	0.0403(9)	0.197(9)
C(73)[b]	0.4811(16)	−0.0607(15)	−0.0016(12)	0.321(18)
N(73)[b]	0.4811(16)	−0.0607(15)	−0.0016(12)	0.321(18)

[a] Equivalent isotropic U defined as one-third of the trace of the orthogonalized U_{ij} tensor ($U_{eq} = {}^1/_3\sum_i\sum_j U_{ij}a_i^*a_j^*a_ia_j$). [b] Disordered positions.

to perform metal-exchange reactions for the sodium.[16] Retention of the Mo_6S_8 cluster unit could be unambiguously proven by the rapid reaction of this pyridine-deficient material with *n*-propylamine and the further ability to form crystalline $Mo_6S_8L_6$ cluster complexes with triethylphosphine, tetrahydrothiophene, pyrrolidine, and piperidine.

(b) Solvent-Exchange Reactions. Crystalline $Mo_6S_8(py)_6$. The pyridine-deficient material was found to be somewhat soluble in pyridine, and upon further reaction in neat pyridine, a brown solid and brown solution were formed. The brown solid from this pyridine reaction was also somewhat pyridine soluble. Greater solubility was observed in other coordinating solvents like *n*-propylamine and piperidine. Coordinated pyridine is evidenced by the characteristic bands in the mid-IR region. The narrow band resulting from the Mo–S stretching vibration at 378 cm⁻¹ indicates that the material has some degree of crystallinity, as further evidenced by several weak lines in the powder X-ray diffraction pattern.

Propylamine. Earlier research found that *n*-propylamine was much more labile than pyridine and thus made an excellent candidate for ligand exchange.[7] The pyridine-deficient material can be readily extracted with *n*-propylamine to form the propylamine adduct. The reaction product appears crystalline; however, it is glassy, as evidenced by an amorphous X-ray diffraction pattern. The amorphous nature is also evidenced in the infrared spectrum of this complex by the broad Mo–S stretching mode centered at 384 cm⁻¹. The XP spectrum shows an absence of sodium, which indicates the removal of sodium sulfide by its remaining on the frit after the extraction.

Pyrrolidine. The pyrrolidine adduct can be easily formed by the substitution of propylamine ligands in neat pyrrolidine; however, single crystals could only be obtained by layering the

(16) Hilsenbeck, S. J.; McCarley, R. E. Manuscript in preparation.

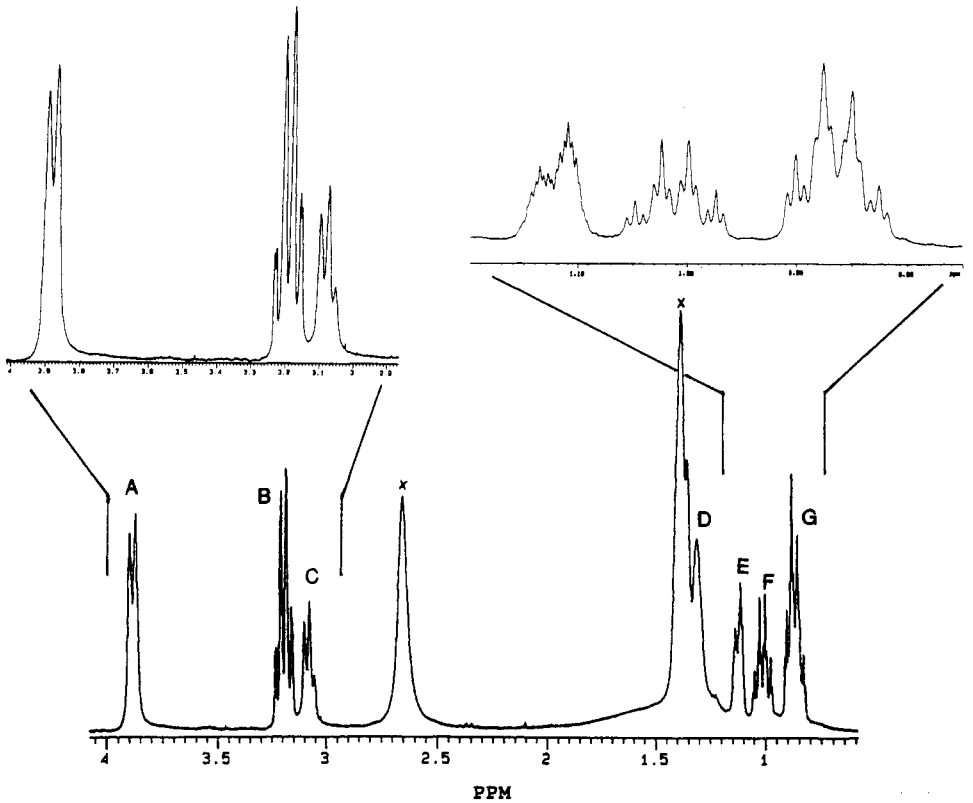

Figure 1. ^{1}H NMR spectrum (500 MHz) of $Mo_6S_8(pip)_6 \cdot x$pip in C_6D_6 solution. The spectrum is labeled as to peak assignments discussed in the text (A–G for coordinated piperidine protons and × for lattice piperidine).

filtrate with diethyl ether. The pyrrolidine adduct was found to be soluble in toluene and is the first readily soluble nitrogen-ligated Mo_6S_8 cluster complex. Over time, some solid slowly precipitates from the toluene solution. Analyses indicate a varying number of pyrrolidines in these complexes with a range of five to seven. An NMR spectrum confirmed the presence of excess pyrrolidine in several samples by showing peaks attributable to both coordinated and lattice pyrrolidine. For free pyrrolidine in deuterated chloroform, the α-CH_2 resonance was reported at 2.78 ppm and the β-CH_2 resonance at approximately 1.60 ppm.[17] The spectrum of the adduct in deuterated benzene shows the lattice ligand α-CH_2 peak at 2.66 ppm and the β-CH_2 peak at 1.41 ppm. Also, broad bands attributable to coordinated pyrrolidine were identified at 1.52 and 0.98 ppm. Further efforts in making proton assignments were not attempted.

Piperidine. The piperidine complex was prepared by the reaction of the propylamine adduct with neat piperidine. By slow reduction of the filtrate volume followed by standing at room temperature, crystalline material is obtained in much larger quantities than for the pyrrolidine adduct. The piperidine adduct is much more soluble than the pyrrolidine complex and exhibits excess lattice piperidine even after drying under dynamic vacuum. This lattice piperidine can be observed by NMR and is indicated by bands in the infrared spectrum near 3100–3200 cm^{-1}. However, drying *in vacuo* results in the significant loss of lattice piperidine, as evidenced by the elemental analyses.

NMR Study on the Piperidine Adduct. The proton spectrum for free piperidine exhibits resonances for α-CH_2 at 2.60 ppm (s) and for β- and γ-CH_2 at 1.38 ppm (s) in deuterated benzene. The 500-MHz NMR spectrum of the piperidine adduct (**5**) is seen in Figure 1. Lattice piperidine peaks are indicated by the ×'s at 2.65 ppm (α-CH_2) and 1.38 ppm (β-, γ-CH_2). The resonances for coordinated piperidine are labeled as A–G and observed in a 2:2:1:2:1:1:2 ratio. The downfield shift of multiplets A and B is consistent with their assignment as α-protons. Likewise, the lower intensities and chemical shifts of E and F are in agreement with γ-proton assignments. The remaining pair of higher intensity peaks, D and G, are assigned as β-protons and peak C is assigned as the proton on the N atom.

The general formula of $Mo_6S_8(pip)_6 \cdot x$pip implies 24 α-H's for coordinated and 4 × α-H's for lattice piperidine. Integration of these α-H resonances suggests 5 equiv of lattice piperidine, which is reasonably close to elemental analyses indicating six piperidine solvate molecules and the crystal structure exhibiting seven. The crystal structure of the piperidine complex shows that the coordinated piperidine adopts a chair conformation and that the ligands are bound to the molybdenum atoms exclusively through equatorial positions. If fast conformational exchange between the boat and chair conformations was occurring in solution, a broadening of the coordinated peaks would be expected due to averaging of the couplings of axial–axial and axial–equatorial protons. This was not observed.

Two-dimensional NMR experiments—DQCOSY (Figure 2) and NOESY (Figure 3)—were undertaken in order to gain further information concerning the proton assignments. The sample prepared for the 2-D NMR experiments exhibited several differences from that of the previous 1-D spectrum (Figure 1), although both samples were prepared from the same reaction product. Residual methanol impurities at δ 3.45–3.32 ppm are indicated by asterisks in Figures 2 and 3. Also, the lattice α-CH_2 peak is of notably reduced intensity and the β and γ resonances for the lattice piperidine are absent in the two-dimensional spectra.

DQCOSY correlations (Table 5) support the assignments made from the 1-D NMR spectrum based on intensities and peak shifts. For example, C is coupled only with A and B, which indicates that it must be the N–H proton. Likewise, A and B interact with C, D, and G, which leads to their assignment as the α-hydrogens. Protons E and F interact only with each other and D and G, which leads to their assignment as the γ-hydrogens. The remaining protons, D and G, are coupled to A, B, D, and E and therefore are β-hydrogens.

(17) Breuer, E.; Melumad, D. *J. Org. Chem.* **1973**, *38*, 1601.

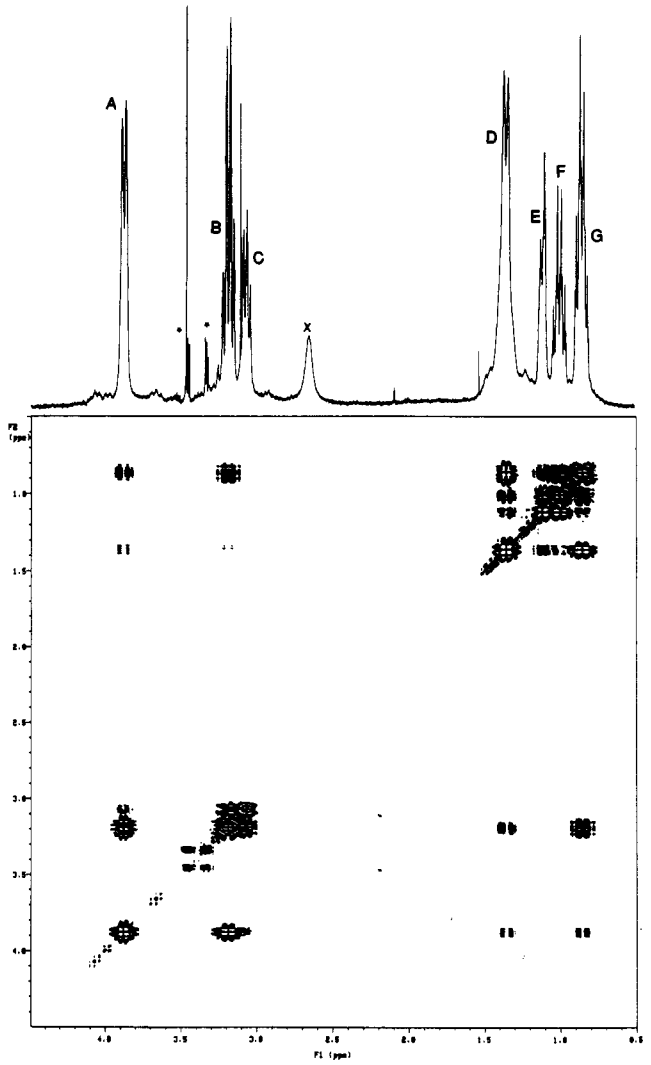

Figure 2. DQCOSY spectrum of $Mo_6S_8(pip)_6 \cdot x$pip showing through-bond interactions. Residual MeOH and lattice piperidine peaks are indicated with an asterisk and ×, respectively.

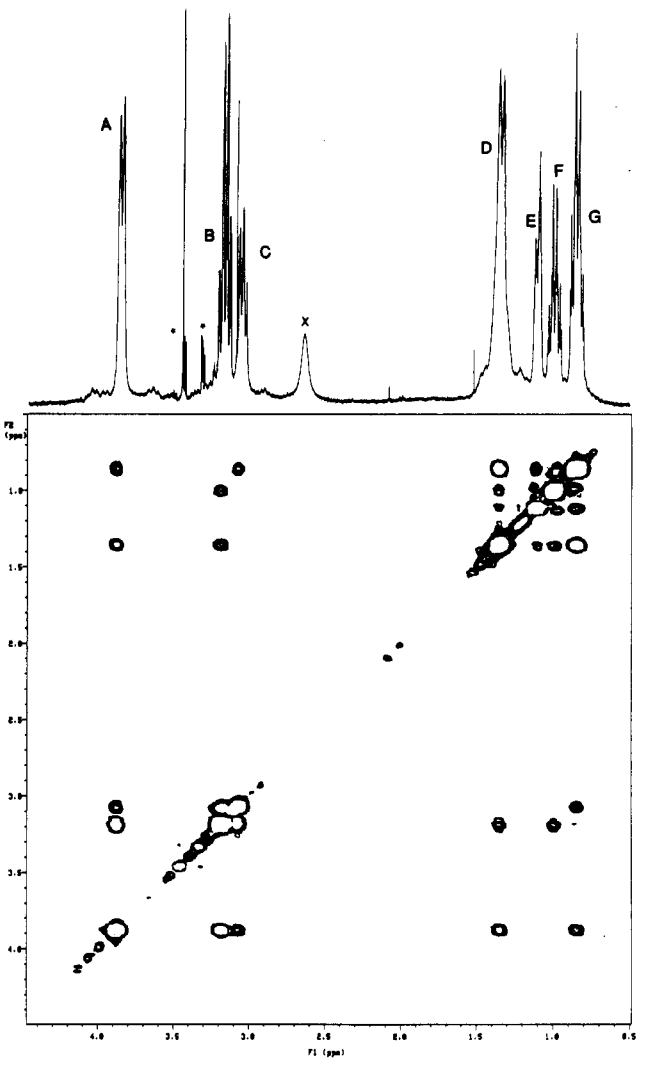

Figure 3. NOESY spectrum of $Mo_6S_8(pip)_6 \cdot x$pip showing through-space interactions. Residual MeOH and lattice piperidine peaks are indicated with an asterisk and ×, respectively.

NOESY interactions (Table 5) further distinguish between the axial and equatorial protons and require the specific assignment shown in the following drawing. The through-space interactions between C and G and between B and F, respectively, confirm their assignment to axial positions.

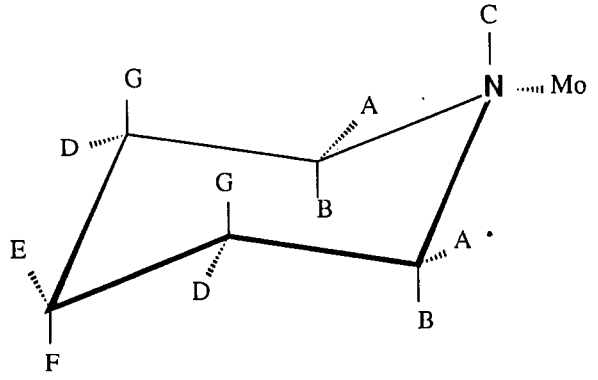

In order to make assignments of the coupling constants, selective decoupling experiments were employed. These results, along with the observation that axial–axial and two-bond couplings are much stronger than equatorial–equatorial or equatorial–axial couplings, allowed for the assignment of the coupling constants reported in the Experimental Section. The observed coupling constants are similar to values found for piperidine complexes with cobalt(III) porphyrin shift reagents.[18] Only the two-bond coupling constants could be resolved for peaks A and D, as seen in Figure 1. All proton couplings can be accounted for by a first-order pattern ABCDEFG, which precludes restricted rotation of the piperidine ligands. If restricted rotation did occur, a second-order splitting pattern AA′BB′CDD′EFGG′ would have been observed.

X-ray Structure Determinations. All the molecular complexes which were prepared contain the hexamolybdenum cluster unit $Mo_6S_8L_6$. This cluster unit can be viewed as an octahedron of molybdenum atoms with eight triply-bridging sulfur atoms capping the octahedral faces. Each molybdenum also possesses an additional coordination site located at the vertex of the octahedron, which is occupied by the nitrogen donor ligands.

The cubic $Mo_6S_8(py)_6 \cdot 2py$ crystallizes in the space group $Pa\bar{3}$ with four molecules per unit cell. Interestingly, this space group was previously observed in the molybdenum sulfide/chloride double salt $(C_5H_5NH)_3[(Mo_6Cl_7S)Cl_6] \cdot 3(C_5H_5NH)Cl$,[19] which also showed $Z = 4$. For the pyridine complex, the hexanuclear unit is a nearly regular octahedron with the average Mo–Mo distance of 2.644(2) Å and a difference between the two symmetry-allowed distances of only 0.006 Å. Selected bond distances and bond angles are listed in Table 6. The Mo_6S_8 cluster unit, shown in Figure 4, is centered on a $\bar{3}$ symmetry axis (4b site symmetry).

(18) Abraham, R. J.; Medforth, C. J. *Magn. Reson. Chem.* **1988**, *26*, 334.
(19) Michel, J. B.; McCarley, R. E. *Inorg. Chem.* **1982**, *21*, 1864.

Table 5. Through-Bond (DQCOSY) and Through-Space (NOESY) Interactions Observed in the Two-Dimensional NMR Spectra Shown in Figures 2 and 3

	A	B	C	D	E	F	G
DQCOSY	B, C, D, G	A, C, D, G	A, B	A, B, E, F, G	D, F, G	D, E, G	A, B, D, E, F
NOESY	B, C, D, G	A, C, D, F	A, B, G	A, B, E, F, G	D, F, G	B, D, E, G	A, C, D, E, F

Table 6. Selected Bond Distances (Å) and Angles (deg) in $Mo_6S_8(py)_6{\cdot}2py$[a]

Mo–Mo(B)	2.641(2)	Mo–N	2.283(9)
Mo–Mo(D)	2.647(2)	N–C(1)	1.34(2)
av Mo–Mo	2.644(2)	N–C(5)	1.32(2)
Mo–S(2)	2.467(3)	C(1)–C(2)	1.34(2)
Mo–S(1A)	2.465(2)	C(2)–C(3)	1.32(2)
Mo–S(2A)	2.461(3)	C(3)–C(4)	1.37(2)
Mo–S(2B)	2.455(3)	C(4)–C(5)	1.38(2)
av Mo–S	2.462(3)		
Mo(B)–Mo–Mo(D)	90.0(1)	S(2)–Mo–N	93.4(2)
Mo(B)–Mo–Mo(E)	60.0(1)	S(1A)–Mo–N	93.1(2)
Mo(D)–Mo–Mo(E)	60.1(1)	S(2A)–Mo–N	93.0(2)
Mo(D)–Mo–Mo(G)	59.9(1)	S(2B)–Mo–N	92.7(2)
S(2)–Mo–S(1A)	90.1(1)	Mo(C)–S(1)–Mo(F)	64.8(1)
S(1A)–Mo–S(2A)	90.2(1)	Mo–S(2)–Mo(D)	65.1(1)
S(2)–Mo–S(2B)	89.4(1)	Mo–S(2)–Mo(E)	64.8(1)
S(2A)–Mo–S(2B)	89.6(1)	Mo(D)–S(2)–Mo(E)	65.1(1)
S(2)–Mo–S(2A)	173.6(1)		
S(1A)–Mo–S(2B)	174.2(1)		

[a] Equivalent atoms generated by symmetry transformations: Mo(B) $-z, {}^1/_2+x, {}^1/_2-y$; Mo(C) $-z, -{}^1/_2+x, -{}^1/_2-y$; Mo(D) $z, {}^1/_2-x, {}^1/_2+y$; Mo(E) ${}^1/_2+y, {}^1/_2-z, -x$; Mo(F) $-{}^1/_2+y, -{}^1/_2-z, -x$; Mo(G) ${}^1/_2-y, {}^1/_2+z, x$; S(1A) $x, {}^1/_2+x, -x$; S(2A) $-z, {}^1/_2+x, {}^1/_2-y$; S(2B) ${}^1/_2-y, {}^1/_2+z, x$.

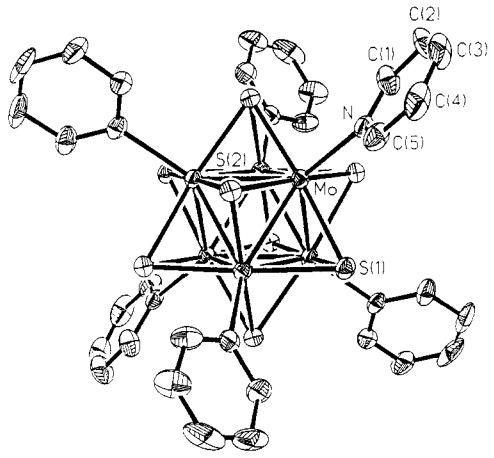

Figure 4. Molecular structure of $Mo_6S_8(py)_6{\cdot}2py$ (**2**). Thermal ellipsoids are shown at the 30% probability level. Hydrogen atoms have been omitted for clarity.

The triclinic form ($Mo_6S_8(py)_6{\cdot}2py$) with two molecules per unit cell was previously observed in the tungsten sulfide cluster complex $W_6S_8(py)_6$[20] and the molybdenum sulfide/chloride complex $Mo_6S_6Cl_2(py)_6$,[6] with only one molecule per unit cell. These latter two complexes are isostructural and contain a much smaller unit cell of about a = 10.7 Å, b = 11.9 Å, and c = 9.4 Å as compared to the triclinic phase with a unit cell of a = 11.6 Å, b = 12.2 Å, and c = 22.0 Å.

The pyrrolidine adduct, $Mo_6S_8(pyrr)_6{\cdot}pyrr$, crystallizes in the tetragonal space group $I4_1/a$ with 16 molecules per unit cell. Two crystallographically independent clusters are found in the asymmetric unit, where cluster 1 is located on a 2-fold position (8e site symmetry) and cluster 2 resides on an inversion center (8d site symmetry). Figures of the two independent asymmetric units are included in the supplementary material. Difficulties were observed in the refinement of the pyrrolidine carbon positions,

(20) Zhang, X. Ph.D. Dissertation, Iowa State University, Ames, IA, 1991.

Table 7. Selected Bond Distances (Å) in $Mo_6S_8(pyrr)_6{\cdot}pyrr$[a]

Mo(11)–Mo(12)	2.645(2)	Mo(21)–Mo(22)	2.645(2)
Mo(11)–Mo(13)	2.663(2)	Mo(21)–Mo(23)	2.642(2)
Mo(11)–Mo(11A)	2.635(2)	Mo(21)–Mo(22B)	2.656(2)
Mo(11)–Mo(13A)	2.646(2)	Mo(21)–Mo(23B)	2.646(2)
Mo(12)–Mo(13)	2.640(2)	Mo(22)–Mo(23)	2.642(2)
Mo(12)–Mo(12A)	2.672(2)	Mo(22)–Mo(23B)	2.644(2)
Mo(12)–Mo(13A)	2.652(1)	av Mo–Mo	2.649(2)
Mo(11)–S(11)	2.440(3)	Mo(21)–S(21)	2.447(4)
Mo(11)–S(12)	2.463(3)	Mo(21)–S(24)	2.441(4)
Mo(11)–S(13)	2.442(3)	Mo(21)–S(22B)	2.445(4)
Mo(11)–S(13A)	2.439(4)	Mo(21)–S(23B)	2.455(4)
Mo(12)–S(11)	2.435(4)	Mo(22)–S(21)	2.439(4)
Mo(12)–S(12)	2.454(3)	Mo(22)–S(22)	2.445(4)
Mo(12)–S(14)	2.457(3)	Mo(22)–S(23)	2.445(4)
Mo(12)–S(14A)	2.448(4)	Mo(22)–S(24)	2.443(4)
Mo(13)–S(12)	2.443(4)	Mo(23)–S(23)	2.455(4)
Mo(13)–S(11A)	2.435(4)	Mo(23)–S(24)	2.449(4)
Mo(13)–S(13A)	2.448(4)	Mo(23)–S(21B)	2.459(4)
Mo(13)–S(14A)	2.455(4)	Mo(23)–S(22B)	2.455(4)
		av Mo–S	2.447(4)
Mo(11)–N(11)	2.278(11)	Mo(21)–N(21)	2.287(11)
Mo(12)–N(12)	2.268(10)	Mo(22)–N(22)	2.269(13)
Mo(13)–N(13)	2.302(11)	Mo(23)–N(23)	2.34(2)
		av Mo–N	2.291(13)

[a] Equivalent atoms A and B generated by symmetry transformations: A $-x, -y+{}^1/_2, z$; B $-x+1, -y+1, -z$.

probably due to solvent loss, which led to the large errors in the observed bond lengths (Table 7) and bond angles (Table 8). The average Mo–Mo bond distance is 2.649(3) Å with a maximum difference between the Mo–Mo distances of 0.030 Å.

The piperidine adduct, $Mo_6S_8(pip)_6{\cdot}7pip$, crystallizes in the tetragonal space group $I\bar{4}$ with eight molecules per unit cell. The Mo_6S_8 cluster unit is centered on a 2-fold position (4e site symmetry). Also, one piperidine solvent molecule is disordered about the same 2-fold position. A diagram of the cluster is shown in Figure 5. The piperidine ligand coordination via equatorial positions can be seen in Figure 6. Selected bond distances and bond angles are listed in Table 9. The average Mo–Mo bond distance is 2.649(1) Å with a maximum difference between these distances of 0.021 Å.

The bond distances for these nitrogen ligand based $Mo_6S_8L_6$ cluster complexes can be compared to those of the rhombohedral triethylphosphine ($R\bar{3}$) and cubic tetrahydrothiophene (tht) ($Ia3$) complexes.[8] A summary of the average bond distances is given in Table 10. The Mo–Mo bond distances of 2.640–2.658 Å and Mo–S distances of 2.430–2.462 Å show only a small spread between these complexes and indicate that the Mo_6S_8 core is relatively unperturbed by the differing ligands. A distinct difference can be noted when the undistorted octahedra in the $Mo_6S_8L_6$ clusters are compared with the trigonally distorted cluster units found in the Chevrel phase compounds.

The octahedra in the Chevrel phases, regardless of electron count, are elongated along the 3-fold axis such that there is a lengthening of the Mo–Mo bonds between the Mo_3 triangles which lie perpendicular to the 3-fold axis. The Mo–Mo bond distances within the Mo_3 triangles range from 2.654 ($ErMo_6S_8$) to 2.698 Å (Mo_6S_8), while the Mo–Mo distances between triangles range from 2.681 ($Cu_{3.66}Mo_6S_8$) to 2.862 Å (Mo_6S_8).[1] This distortion results from a close approach between cluster units and formation of weak intercluster Mo–Mo bonds, as evidenced by the distance (6×) of 3.084 Å for the highly distorted Mo_6S_8. Of course, the isolated $Mo_6S_8L_6$ cluster units show no intercluster Mo–Mo bonding and negligible distortion of the octahedron. The Chevrel

Table 8. Selected Bond Angles (deg) in $Mo_6S_8(pyrr)_6 \cdot pyrr$[a]

Mo(12)–Mo(11)–Mo(13)	59.6(1)	Mo(22)–Mo(21)–Mo(23)	60.0(1)
Mo(12)–Mo(11)–Mo(13A)	60.1(1)	Mo(22)–Mo(21)–Mo(23B)	60.0(1)
Mo(13)–Mo(11)–Mo(11A)	59.9(1)	Mo(23)–Mo(21)–Mo(22B)	59.9(1)
Mo(11A)–Mo(11)–Mo(13A)	60.6(1)	Mo(22B)–Mo(21)–Mo(23B)	59.8(1)
Mo(11)–Mo(12)–Mo(13)	60.5(1)	Mo(21)–Mo(22)–Mo(23)	60.0(1)
Mo(11)–Mo(12)–Mo(13A)	59.9(1)	Mo(21)–Mo(22)–Mo(23B)	60.0(1)
Mo(13)–Mo(12)–Mo(12A)	59.9(1)	Mo(23)–Mo(22)–Mo(21B)	59.9(1)
Mo(12A)–Mo(12)–Mo(13A)	59.4(1)	Mo(21B)–Mo(22)–Mo(23B)	59.8(1)
Mo(11)–Mo(13)–Mo(12)	59.8(1)	Mo(21)–Mo(23)–Mo(22)	60.1(1)
Mo(11)–Mo(13)–Mo(11A)	59.5(1)	Mo(21)–Mo(23)–Mo(22B)	60.3(1)
Mo(12)–Mo(13)–Mo(12A)	60.6(1)	Mo(22)–Mo(23)–Mo(21B)	60.3(1)
Mo(11A)–Mo(13)–Mo(12A)	59.9(1)	Mo(21B)–Mo(23)–Mo(22B)	60.0(1)
		av Mo–Mo–Mo	60.0(1)
Mo(12)–Mo(11)–Mo(11A)	90.4(1)	Mo(22)–Mo(21)–Mo(22B)	90.0(1)
Mo(13)–Mo(11)–Mo(13A)	89.8(1)	Mo(23)–Mo(21)–Mo(23B)	89.7(1)
Mo(11)–Mo(12)–Mo(12A)	89.6(1)	Mo(21)–Mo(22)–Mo(21B)	90.0(1)
Mo(13)–Mo(12)–Mo(13A)	90.2(1)	Mo(23)–Mo(22)–Mo(23B)	89.7(1)
Mo(11)–Mo(13)–Mo(12A)	89.6(1)	Mo(21)–Mo(23)–Mo(21B)	90.3(1)
Mo(12)–Mo(13)–Mo(11A)	90.3(1)	Mo(22)–Mo(23)–Mo(22B)	90.3(1)
		av Mo–Mo–Mo	90.0(1)
Mo(11)–S(11)–Mo(12)	65.7(1)	Mo(21)–S(21)–Mo(22)	65.6(1)
Mo(11)–S(11)–Mo(13A)	65.7(1)	Mo(21)–S(21)–Mo(23B)	65.3(1)
Mo(12)–S(11)–Mo(13A)	66.0(1)	Mo(22)–S(21)–Mo(23B)	65.3(1)
Mo(11)–S(12)–Mo(13)	65.8(1)	Mo(22)–S(22)–Mo(21B)	65.8(1)
Mo(11)–S(12)–Mo(12)	65.1(1)	Mo(22)–S(22)–Mo(23B)	65.3(1)
Mo(12)–S(12)–Mo(13)	65.2(1)	Mo(21B)–S(22)–Mo(23B)	65.2(1)
Mo(11)–S(13)–Mo(11A)	65.4(1)	Mo(22)–S(23)–Mo(21B)	65.7(1)
Mo(11)–S(13)–Mo(13A)	65.5(1)	Mo(22)–S(23)–Mo(23)	65.2(1)
Mo(11A)–S(13)–Mo(13A)	66.0(1)	Mo(23)–S(23)–Mo(21B)	65.2(1)
Mo(12)–S(14)–Mo(12A)	66.0(1)	Mo(21)–S(24)–Mo(22)	65.6(1)
Mo(12)–S(14)–Mo(13A)	65.4(1)	Mo(21)–S(24)–Mo(23)	65.4(1)
Mo(12A)–S(14)–Mo(13A)	65.1(1)	Mo(22)–S(24)–Mo(23)	65.4(1)
		av Mo–S–Mo	65.5(1)
S(11)–Mo(11)–S(12)	90.2(1)	S(21)–Mo(21)–S(24)	89.5(2)
S(11)–Mo(11)–S(13)	90.1(1)	S(21)–Mo(21)–S(23B)	90.4(2)
S(12)–Mo(11)–S(13A)	88.4(1)	S(24)–Mo(21)–S(22B)	90.3(2)
S(13)–Mo(11)–S(13A)	90.4(2)	S(22B)–Mo(21)–S(23B)	89.1(2)
S(11)–Mo(12)–S(12)	90.5(1)	S(21)–Mo(22)–S(22)	90.3(2)
S(11)–Mo(12)–S(14)	89.8(1)	S(21)–Mo(22)–S(24)	89.6(2)
S(12)–Mo(12)–S(14A)	90.5(1)	S(22)–Mo(22)–S(23)	89.3(1)
S(14)–Mo(12)–S(14A)	88.3(1)	S(23)–Mo(22)–S(24)	90.1(2)
S(12)–Mo(13)–S(13A)	88.6(1)	S(23)–Mo(23)–S(24)	89.7(1)
S(12)–Mo(13)–S(14A)	90.6(1)	S(23)–Mo(23)–S(21B)	90.1(1)
S(11A)–Mo(13)–S(13A)	90.1(1)	S(24)–Mo(23)–S(22B)	89.8(1)
S(11A)–Mo(13)–S(14A)	89.8(1)	S(21B)–Mo(23)–S(22B)	89.6(1)
		av S–Mo–S	89.8(1)
S(11)–Mo(11)–S(13A)	173.0(1)	S(21)–Mo(21)–S(22B)	173.2(1)
S(12)–Mo(11)–S(13)	173.0(1)	S(24)–Mo(21)–S(23B)	173.2(1)
S(11)–Mo(12)–S(14A)	173.0(1)	S(21)–Mo(22)–S(23)	173.6(1)
S(12)–Mo(12)–S(14)	173.0(1)	S(24)–Mo(22)–S(22)	173.3(1)
S(12)–Mo(13)–S(11A)	173.4(1)	S(23)–Mo(23)–S(22B)	173.2(2)
S(13A)–Mo(13)–S(14A)	172.8(1)	S(24)–Mo(23)–S(21B)	173.3(2)
		av S–Mo–S	173.2(1)
S(11)–Mo(11)–N(11)	95.7(3)	S(21)–Mo(21)–N(21)	96.0(3)
S(12)–Mo(11)–N(11)	97.5(3)	S(24)–Mo(21)–N(21)	96.2(3)
S(13)–Mo(11)–N(11)	89.5(3)	S(22B)–Mo(21)–N(21)	90.7(3)
S(13A)–Mo(11)–N(11)	91.3(3)	S(23B)–Mo(21)–N(21)	90.6(3)
S(11)–Mo(12)–N(12)	94.2(3)	S(21)–Mo(22)–N(22)	94.9(4)
S(12)–Mo(12)–N(12)	89.9(3)	S(22)–Mo(22)–N(22)	90.9(4)
S(14)–Mo(12)–N(12)	97.0(3)	S(23)–Mo(22)–N(22)	91.4(4)
S(14A)–Mo(12)–N(12)	92.7(3)	S(24)–Mo(22)–N(22)	95.7(4)
S(12)–Mo(13)–N(13)	90.9(3)	S(23)–Mo(23)–N(23)	94.7(5)
S(11A)–Mo(13)–N(13)	95.7(3)	S(24)–Mo(23)–N(23)	91.3(5)
S(13A)–Mo(13)–N(13)	96.6(3)	S(21B)–Mo(23)–N(23)	95.5(5)
S(14A)–Mo(13)–N(13)	90.6(3)	S(22B)–Mo(23)–N(23)	92.1(5)
		av S–Mo–N	93.4(3)

[a] Equivalent atoms A and B generated by symmetry transformations: A $-x, -y + 1/2, z$; B $-x + 1, -y + 1, -z$.

phases exhibit average Mo–S distances of about 2.44–2.46 Å, which are very similar to the distances observed for the $Mo_6S_8L_6$ cluster units.

The application of bond order calculations has proven useful in understanding the stability of the cluster unit relative to the loss of ligands. The bond order for metal–metal or metal–ligand bonds can be determined by using Pauling's bond order equation[21]

$$d(n) = d(1) - 0.6 \log n$$

where $d(n)$ is the observed bond distance, $d(1)$ is the single-bond distance, and n is the bond order. The calculations for the Mo–

(21) Pauling, L. *The Nature of the Chemical Bond*, 3rd ed.; Cornell University Press: Ithaca, NY, 1960; p 400.

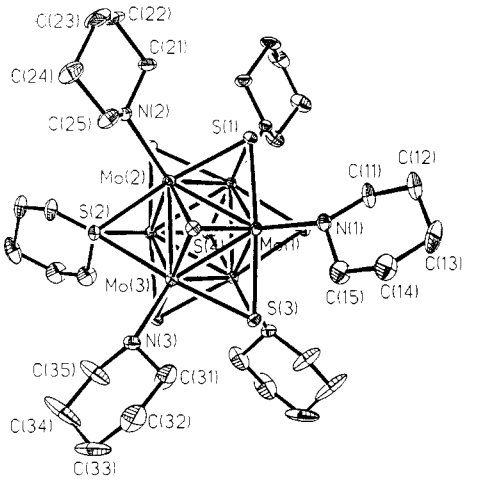

Figure 5. Molecular structure of $Mo_6S_8(pip)_6 \cdot 7pip$ (**5**). Thermal ellipsoids are shown at the 30% probability level. Hydrogen atoms have been omitted for clarity.

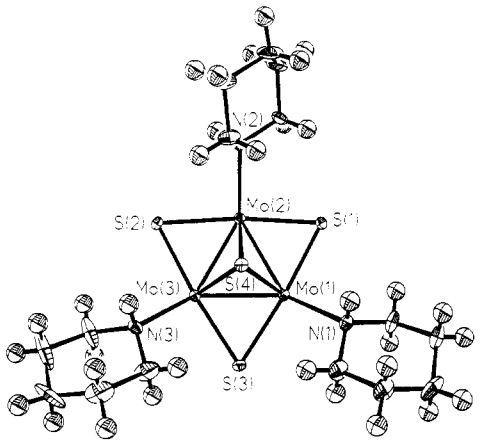

Figure 6. View of $Mo_6S_8(pip)_6 \cdot 7pip$ (**5**) showing the equatorial coordination of the piperidine ligands to the Mo_6S_8 cluster unit. Thermal ellipsoids are shown at the 30% probability level.

Mo and Mo–L bond orders are given in Table 10. The calculated Mo–Mo bond distance, $d(n)$, for the Mo_6S_8 unit with average bond order $n = {}^{20}/_{24} = 0.833$ is 2.662 Å, where $d(1) = 2.614$ Å is used as the Mo–Mo single-bond value. From the observed distances, all of which are a little shorter than this expected distance, the calculated bond orders are a little high, within the range 0.846–0.907. However, these values are still in reasonable agreement with the expected value of 0.833 for the 20-electron cluster compounds.

The Mo–S single-bond distance was arbitrarily taken as 2.44 Å, the average of the Mo–S distances in the $Mo_6S_8L_6$ cluster unit. From this result, a value of 1.40 Å was obtained for the covalent radius of Mo. Bond order calculations for the Mo–L bonds indicate that the strengths of the bondings between the cluster and coordinated ligands differ significantly depending upon the terminal ligand. The bond order for the Mo–P bond of the triethylphosphine adduct is much greater than those for the Mo–S or Mo–N bonds for the sulfur- or nitrogen-ligand complexes. Also, it is noted that the nitrogen-based ligands, piperidine in particular, show the weakest Mo–L bonding and thus should be the easiest ligands to remove upon deligation.

Raman Spectroscopy. The technique of Raman spectroscopy was utilized in order to gain information about the Mo_6S_8 cluster complexes prior to and after deligation.[16] Initial interest focused on the crystalline piperidine complex. In this spectrum (Figure 7), the most distinguishing feature is the sharp peak at 411 cm^{-1}, which can be attributed to the A_{1g} totally symmetric Mo–S stretching mode. This peak assignment is suggested by the reported assignments for MoS_2 at 409 (A_{1g}), 383 (E^1_{2g}), 287 (E_{1g}), and 118 (E^2_{2g}) cm^{-1}.[22]

The Raman spectra for several Chevrel phases have been reported.[23] However, the rhombohedral symmetry and strong Mo–S–Mo intercluster bridge bonding in the Chevrel phase compounds preclude any obvious correspondence for the Raman bands with those found here in the discrete molecular cluster derivatives. In particular, there appears to be no single band in the spectra of the Chevrel phases which corresponds directly to the intense, totally symmetric Mo–S A_{1g} breathing mode of the isolated molecular clusters. The two strongest bands in the Chevrel phase spectra occur in the ranges 236–250 and 282–305 cm^{-1} and are suggested as A_g modes though no description is given regarding the specific vibrations involved.

In any case, the predominant band in the spectra of these molecular complexes occurs in the 411–418-cm^{-1} region, as typified by the spectrum in Figure 7. Other bands are noted at 457, 273, and 259 cm^{-1} in this spectrum, but their assignment is obscure. The broad band at 836 cm^{-1} is most likely the first

Table 9. Selected Bond Distances (Å) and Angles (deg) in $Mo_6S_8(pip)_6 \cdot 7pip$[a]

Mo(1)–Mo(2)	2.652(1)	Mo(1)–S(1)	2.448(2)
Mo(1)–Mo(3)	2.640(1)	Mo(1)–S(3)	2.446(2)
Mo(1)–Mo(2A)	2.653(1)	Mo(1)–S(4)	2.456(1)
Mo(1)–Mo(3A)	2.653(1)	Mo(1)–S(2A)	2.460(1)
Mo(2)–Mo(3)	2.658(1)	Mo(2)–S(1)	2.463(2)
Mo(2)–Mo(2A)	2.637(1)	Mo(2)–S(2)	2.456(2)
Mo(3)–Mo(3A)	2.652(1)	Mo(2)–S(4)	2.465(2)
av Mo–Mo	2.649(1)	Mo(2)–S(1A)	2.448(2)
Mo(1)–N(1)	2.322(4)	Mo(3)–S(2)	2.452(2)
Mo(2)–N(2)	2.321(5)	Mo(3)–S(3)	2.444(2)
Mo(3)–N(3)	2.308(5)	Mo(3)–S(4)	2.456(2)
av Mo–N	2.317(5)	Mo(3)–S(3A)	2.431(2)
		av Mo–S	2.452(2)
Mo(2)–Mo(1)–Mo(3)	60.3(1)	S(1)–Mo(1)–S(4)	90.0(1)
Mo(2)–Mo(1)–Mo(2A)	59.6(1)	S(3)–Mo(1)–S(4)	90.6(1)
Mo(3)–Mo(1)–Mo(3A)	60.1(1)	S(1)–Mo(1)–S(2A)	89.4(1)
Mo(2A)–Mo(1)–Mo(3A)	60.1(1)	S(3)–Mo(1)–S(2A)	89.3(1)
Mo(1)–Mo(2)–Mo(3)	59.6(1)	S(1)–Mo(2)–S(4)	89.4(1)
Mo(3)–Mo(2)–Mo(1A)	60.0(1)	S(2)–Mo(2)–S(4)	89.3(1)
Mo(1)–Mo(2)–Mo(2A)	60.2(1)	S(1)–Mo(2)–S(1A)	91.0(1)
Mo(1A)–Mo(2)–Mo(2A)	60.2(1)	S(2)–Mo(2)–S(1A)	89.5(1)
Mo(1)–Mo(3)–Mo(2)	60.1(1)	S(2)–Mo(3)–S(4)	89.6(1)
Mo(2)–Mo(3)–Mo(1A)	59.9(1)	S(3)–Mo(3)–S(4)	90.6(1)
Mo(1)–Mo(3)–Mo(3A)	60.2(1)	S(2)–Mo(3)–S(3A)	89.8(1)
Mo(1A)–Mo(3)–Mo(3A)	59.7(1)	S(3)–Mo(3)–S(3A)	89.1(1)
av Mo–Mo–Mo	60.0(1)	av S–Mo–S	89.8(1)
Mo(3)–Mo(1)–Mo(2A)	90.2(1)	S(1)–Mo(1)–S(3)	173.3(1)
Mo(2)–Mo(1)–Mo(3A)	89.9(1)	S(4)–Mo(1)–S(2A)	173.3(1)
Mo(1)–Mo(2)–Mo(1A)	89.8(1)	S(1)–Mo(2)–S(2)	173.0(1)
Mo(3)–Mo(2)–Mo(2A)	90.2(1)	S(4)–Mo(2)–S(1A)	173.5(1)
Mo(1)–Mo(3)–Mo(1A)	90.1(1)	S(2)–Mo(3)–S(3)	173.0(1)
Mo(2)–Mo(3)–Mo(3A)	89.8(1)	S(4)–Mo(3)–S(3A)	173.6(1)
av Mo–Mo–Mo	90.0(1)	av S–Mo–S	173.3(1)
Mo(1)–S(1)–Mo(2)	65.4(1)	S(1)–Mo(1)–N(1)	90.6(2)
Mo(1)–S(1)–Mo(2A)	65.6(1)	S(3)–Mo(1)–N(1)	96.1(2)
Mo(2)–S(1)–Mo(2A)	64.9(1)	S(4)–Mo(1)–N(1)	89.3(1)
Mo(2)–S(2)–Mo(3)	65.6(1)	S(2A)–Mo(1)–N(1)	97.3(1)
Mo(2)–S(2)–Mo(1A)	65.3(1)	S(1)–Mo(2)–N(2)	94.0(1)
Mo(3)–S(2)–Mo(1A)	65.4(1)	S(2)–Mo(2)–N(2)	93.0(1)
Mo(1)–S(3)–Mo(3)	65.4(1)	S(4)–Mo(2)–N(2)	97.6(1)
Mo(1)–S(3)–Mo(3A)	65.9(1)	S(1A)–Mo(2)–N(2)	88.9(1)
Mo(3)–S(3)–Mo(3A)	65.9(1)	S(2)–Mo(3)–N(3)	92.7(1)
Mo(1)–S(4)–Mo(2)	65.2(1)	S(3)–Mo(3)–N(3)	94.4(1)
Mo(1)–S(4)–Mo(3)	65.0(1)	S(4)–Mo(3)–N(3)	91.5(1)
Mo(2)–S(4)–Mo(3)	65.4(1)	S(3A)–Mo(3)–N(3)	94.8(1)
av Mo–S–Mo	65.4(1)	av S–Mo–N	93.4(1)

[a] Equivalent atoms generated by symmetry transformation: A $-x, -y, z$.

(22) Verble, J. L.; Wieting, T. J. *Phys. Rev. Lett.* **1970**, *25*, 362.
(23) Holmgren, D. J.; Demers, R. T.; Klein, M. V.; Ginsberg, D. M. *Phys. Rev. B* **1987**, *36*, 1952.

Table 10. Bond Distances (Å) and Bond Order Calculations for the $Mo_6S_8L_6$ Cluster Complexes

formula	Mo–Mo	Mo–S	Mo–L	est Mo–L[a]	BO(Mo–Mo)[b]	BO(Mo–L)[c]
$Mo_6S_8(PEt_3)_6 \cdot 2DCM$[d]	2.6584(5)	2.446(1)	2.524(1)	2.50	0.846(2)	0.913(4)
$Mo_6S_8(tht)_6$	2.640(4)	2.430(8)	2.576(8)	2.44	0.907(14)	0.60(2)
$Mo_6S_8(py)_6 \cdot 2py$	2.644(2)	2.462(3)	2.283(9)	2.10	0.893(7)	0.50(2)
$Mo_6S_8(pip)_6 \cdot 7pip$	2.649(1)	2.454(2)	2.317(5)	2.10	0.876(3)	0.43(1)
$Mo_6S_8(pyrr)_6 \cdot pyrr$	2.648(2)	2.447(4)	2.291(13)	2.10	0.878(6)	0.48(2)

[a] Estimated single-bond distance from Pauling covalent radii r(N), r(S), and r(Mo). The value of r(Mo) = 1.40 Å was estimated from r(Mo) = d(Mo–S) – r(S), where d(Mo–S) is the average value 2.44 Å from the table. [b] Estimated bond order from the Pauling bond order equation, $d(n) = d(1) - 0.6 \log n$, where $d(n)$ is the observed Mo–Mo distance and $d(1)$ is the estimated Mo–Mo single-bond distance, 2.614 Å. [c] Estimated bond order from the Pauling bond order equation, $d(n) = d(1) - 0.6 \log n$, where $d(n)$ is the observed Mo–L distance and $d(1)$ is the estimated Mo–L single-bond distance. [d] DCM = dichloromethane.

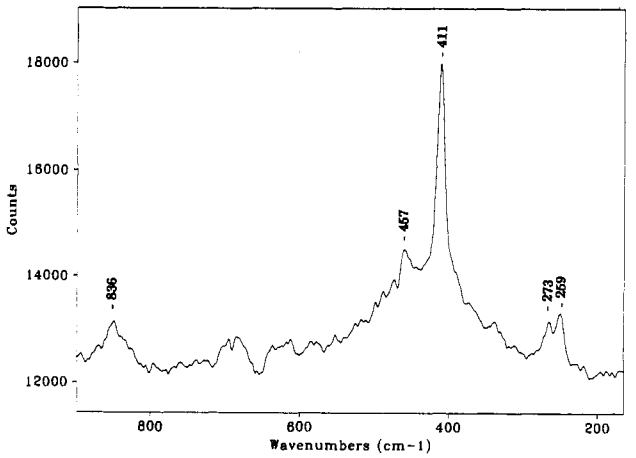

Figure 7. Raman spectrum of the piperidine adduct exhibiting the sharp Mo–S A_{1g} mode at 411 cm^{-1} characteristic of a crystalline $Mo_6S_8L_6$ cluster complex.

Table 11. Infrared and Raman Frequencies (cm^{-1}) for the Cluster Complexes

	infrared ν(Mo–S)	Raman Mo–S A_{1g} mode
$Mo_6S_8(PEt_3)_6$	390	416
$Mo_6S_8(tht)_6$	389	416
$Mo_6S_8(pip)_6$	382	411
$Mo_6S_8(pyrr)_6$	381	415
$Mo_6S_8(PrNH_2)_{6-x}$	384 (br)	448 (br)
$Mo_6S_8(py)_6$	378	418
$Na_{2x}Mo_6S_{8+x}(py)_y$	392 (br)	448 (br)

overtone of the band at 411 cm^{-1}. It is reasonable to expect that the totally symmetric cluster breathing mode (perhaps mixed Mo–S and Mo–Mo) should entail the greatest change in polarizability and thus appear as the most intense Raman transition. Further assessment of possible assignments must await more extensive study of both Raman and infrared spectra.

Table 11 lists the intense IR and Raman bands assigned as the Mo–S modes. As noted in this table, all of the $Mo_6S_8L_6$ cluster complexes show the presence of the A_{1g} mode at 411–418 cm^{-1}; however, as ligands are lost, a broadening can be observed. The ligand-deficient propylamine and pyridine cluster complexes exhibit a broadened Mo–S band with the peak center at 448 cm^{-1} in the Raman spectra. The loss of ligands and possible formation of intercluster bonds would destroy the octahedral symmetry which produced the A_{1g} mode, and thus this mode is absent. However, this broad band is indicative of the cluster unit as supported by other spectroscopic techniques (IR, XPS) and can be used as a means of identifying the presence of the Mo_6S_8 cluster unit upon further deligation reactions.

X-ray Photoelectron Spectroscopy. XPS was used to obtain Mo and S binding energies and further information about possible cluster degradation. If decomposition did occur to form MoS_2 and Mo metal during the reactions, distinct differences would be found in the binding energy values. The results of the XPS study are tabulated in Table 12. The only reported Mo_6S_8 cluster complex, $Mo_6S_8(PEt_3)_6$, showed molybdenum binding energies at 227.8 ($3d_{5/2}$) and 231.0 eV ($3d_{3/2}$) and sulfur binding energies at 161.1 ($2p_{3/2}$) and 162.1 eV ($2p_{1/2}$).[24] The cluster complexes reported in this work all exhibit Mo $3d_{5/2}$ values between 227.6 and 227.8 eV and Mo $3d_{3/2}$ values between 230.7 and 230.9 eV. These values are slightly lower than those reported for the triethylphosphine adduct but are still very close to each other. Likewise, the sulfur binding energies are very similar where the S $2p_{3/2}$ values lie between 160.6 and 161.0 eV and the S $2p_{1/2}$ values, taken from the shoulders, lie between 161.8 and 162.1 eV. The sulfur 2s binding energies are also in a narrow range of 224.9–225.4 eV. These results are similar to the values observed for the Chevrel phases which range from 227.3 to 228.2 eV for the Mo $3d_{5/2}$ peak.[4b,25] However, noticeable differences exist when comparison is made to MoS_2, a decomposition product. The MoS_2 binding energies for molybdenum are found to be 229.5 ($3d_{5/2}$) and 232.6 eV ($3d_{3/2}$). The values for sulfur are 226.7 (2s), 162.3 ($2p_{3/2}$), and 163.5 eV ($2p_{1/2}$). These binding energies for MoS_2 are similar to values that have been previously reported.[26]

Table 12. XPS Binding Energies (eV) for the Mo_6S_8 Cluster Complexes[a]

	$(pip)_6$	$(pyrr)_6$	$(py)_6$	$(PrNH_2)_{6-x}$[b]	$(PEt_3)_6$	$(tht)_6$
Mo $3d_{5/2}$	227.7	227.7	227.6	227.7	227.8	227.7
Mo $3d_{3/2}$	230.8	230.8	230.7	230.9	230.9	230.9
S 2s	224.9	225.4	225.0	225.3	225.1	225.2
S $2p_{3/2}$	160.7	160.6	160.6	160.6	161.0	160.7
S $2p_{1/2}$[c]	161.9	161.8	161.8	161.8	162.1	161.8

[a] Data have been corrected to the C 1s binding energy of 284.6 eV. [b] The propylamine adduct is ligand-deficient. [c] This peak is evidenced as a shoulder on the main S $2p_{3/2}$ peak.

Conclusions

This paper describes the preparation and characterization of new molecular $Mo_6S_8L_6$ cluster complexes. In an attempt to improve the two-step preparative route to the completely sulfur-substituted cluster "$Mo_6S_8(py)_y$", it was discovered that this compound had been misformulated. Both the previous two-step route and the modified one-step method with higher stoichiometric amounts of the sulfiding agent, NaSH, result in a similar product which contains sodium, $Na_{2x}Mo_6S_{8+x}(py)_y$. For this procedure, the pyridine content was found to be somewhat variable and dependent upon the reaction conditions.

This pyridine-deficient material is quite amenable to undergoing ligand-exchange reactions. Further reaction in neat pyridine produces the crystalline hexapyridine complex, which exists in both the cubic and triclinic forms. Reaction of the pyridine-deficient material with *n*-propylamine results in the formation of the reactive propylamine adduct. The weakly bound propylamine ligands allow for facile ligand exchange and the preparation of new complexes with pyrrolidine and piperidine. These adducts

(24) Saito, T.; Yamamoto, N.; Nagase, T.; Tsuboi, T.; Kobayashi, K.; Yamagata, T.; Imoto, H.; Unoura, K. *Inorg. Chem.* **1990**, *29*, 764.
(25) Yashonath, S.; Hegde, M. S.; Sarode, P. R.; Rao, C. N. R.; Umarji, A. M.; Subba Rao, G. V. *Solid State Commun.* **1981**, *37*, 325.
(26) Stevens, G. C.; Edmonds, T. *J. Catal.* **1975**, *37*, 544.

crystallize in tetragonal space groups. Also, they are soluble in organic solvents, which allows for study by NMR spectroscopy. The complexes show spectra consistent with the presence of both coordinated and lattice ligands. Two-dimensional NMR studies on the piperidine adduct have resulted in assignments for the protons. Also, the structural results show that the piperidine ligands are coordinated via equatorial positions.

Information has been gained from Raman and XP spectra of these molecular $Mo_6S_8L_6$ complexes in addition to the more standard elemental analyses and infrared spectra. Characteristic bands can be detected in the Raman and XP spectra which corroborate the presence of the Mo_6S_8 cluster unit. Structural information on these nitrogen-ligated complexes has shown them to possess the weakest Mo–L bonds, as evidenced in their relatively low Mo–N bond orders. The results indicate that these complexes should be the best materials for further deligation studies to prepare the Chevrel phase compounds.[16]

Acknowledgment. We wish to thank James Anderegg for aid with the XP spectra, Jeanne Wynn for help with the Raman spectra, David Scott for aid in collecting the NMR spectra, and James R. Martin for help in interpreting the NMR data. This work was supported by the U.S. Department of Energy, Office of Basic Energy Sciences, through Ames Laboratory operated by Iowa State University under Contract No. W-7405-Eng-82.

Supplementary Material Available: Listings of complete crystallographic parameters, bond distances, bond angles, H atom positions, and anisotropic temperature factors and figures showing unit cell arrangements (39 pages). Ordering information is given on any current masthead page.